

## Laser based impedance measurement for pipe corrosion and bolt-loosening detection

Jinyeol Yang, Peipei Liu, Suyoung Yang, Hyeonseok Lee and Hoon Sohn\*

*Department of Civil Engineering, Korea Advanced Institute for Science and Technology,  
291 Daehak-ro, Yuseong-gu, Daejeon 305-701, Republic of Korea*

*(Received November 20, 2013, Revised December 20, 2014, Accepted January 17, 2014)*

**Abstract.** This study proposes a laser based impedance measurement system and impedance based pipe corrosion and bolt-loosening monitoring techniques under temperature variations. For impedance measurement, the laser based impedance measurement system is optimized and adopted in this paper. First, a modulated laser beam is radiated to a photodiode, converting the laser beam into an electric signal. Then, the electric signal is applied to a MFC transducer attached on a target structure for ultrasonic excitation. The corresponding impedance signals are measured, re-converted into a laser beam, and radiated back to the other photodiode located in a data interrogator. The transmitted impedance signals are treated with an outlier analysis using generalized extreme value (GEV) statistics to reliably signal off structural damage. Validation of the proposed technique is carried out to detect corrosion and bolt-loosening in lab-scale carbon steel elbow pipes under varying temperatures. It has been demonstrated that the proposed technique has a potential to be used for structural health monitoring (SHM) of pipe structures.

**Keywords:** structural health monitoring; impedance; laser; wireless data transmission; outlier analysis; macro-fiber composite; temperature compensation; carbon steel elbow pipe; corrosion; bolt-loosening

### 1. Introduction

The world heavily depends on a vast network of pipeline systems for transporting and distributing natural resources such as oil and natural gas across thousands of miles. The structural conditions of pipeline systems continue to deteriorate, and several accidents associated with pipeline structures took place over the past years, resulting in human casualties and property losses (Papadakis 1999, Azevedo 2007). Pipes are particularly vulnerable to corrosion because of the fluid flowing inside the pipes and their continuous operation under corrosive environments (Lawson 2005). Another critical damage type is bolt-loosening at pipe joints caused by pipe vibration and corrosion of bolts and nuts. To prevent such catastrophic failures, the industries invested in pipeline infrastructure have tightened their safety measures and are adopting structural health monitoring (SHM) techniques to operational pipeline facilities as a supplement to conventional safety measures.

Among various SHM approaches, an impedance technique has been recognized as one of the

---

\*Corresponding author, Professor, E-mail: [hoonsohn@kaist.ac.kr](mailto:hoonsohn@kaist.ac.kr)

promising methods for detecting initial damage (Chaudhry and Ganino 1994, Ayres *et al.* 1998, Zou *et al.* 2000, Bhalla and Soh 2004, Grisso and Inman 2008). The impedance signals are measured by a single piezoelectric transducer attached onto a host structure. Here, the piezoelectric transducer acts as both an actuator and a sensor, and extracts a high-frequency modal spectrum of the host structure. Impedance techniques are attractive for various SHM applications because (a) they are sensitive to various sizes of structural damage, and (b) a relatively simple hardware configuration is required compared to other SHM systems (Giurgiutiu and Zagrai 2002). A number of impedance techniques have been developed for SHM applications. Giurgiutiu and Zagrai (Giurgiutiu and Zagrai 2005) used an impedance technique to detect damage in thin metallic plates. Kim *et al.* (2011) developed a baseline-free impedance method for crack detection in thin plate-like structure. Because conventional piezoelectric materials such as lead zirconate titanate (PZT) are brittle, macro-fiber composite (MFC) transducers, which are conformable to curved surface, are used for impedance measurement of pipe structures (Hamzeloo *et al.* 2012). For straight pipeline structures, impedance based techniques were studied to detect corrosion damage (Zhang *et al.* 2012) and bolt-loosening (Thien *et al.* 2007). Krishnamurthy *et al.* developed a temperature compensation technique by using temperature coefficients (Krishnamurthy *et al.* 1996). Lim *et al.* used cross-correlation and Kernel principal component analysis to compensate frequency shifting caused by temperature variation (Lim *et al.* 2011). Recently, wireless impedance measurement systems also have been developed (Mascarenas *et al.* 2007, Min *et al.* 2010).

This study presents a laser based impedance measurement system that can be used for continuous monitoring of corrosion and bolt-loosening damages in pipe structures. Laser sources and optoelectronic devices are optimized to generate and measure impedance signals using MFC transducers. The MFC transducers are attached to a curved specimen to generate and measure the impedance signals for damage detection. Then, an outlier analysis using generalized extreme value (GEV) statistics is applied to measurement of the impedance signals for automated damage diagnosis at the presence of temperature variations. The feasibility of the proposed technique is verified using test data obtained from varying temperature conditions of elbow pipes with corrosion and bolt-loosening.

This paper is organized as follows. In section 2, the proposed impedance measurement technique with the outlier analysis using GEV statistics is described considering temperature effect compensation. In section 3, the principle of the laser based impedance measurement system is described, and the hardware development and its verification are presented as well. Experimental test results from corrosion and bolt-loosening damage states are reported in sections 4 and 5. This paper concludes with a summary and discussions in section 6.

## 2. Impedance based damage detection

In this study, MFC transducers are used instead of PZT transducers because PZT transducers are brittle and unconformable to curved surfaces. For impedance measurement, a MFC transducer is mounted on a host structure and an input voltage is applied to the MFC transducer. Then, the resulting output current is measured, and the electrical impedance is defined as the ratio of the input voltage to the output current. Here, the mechanical impedances of the MFC itself and the host structure are coupled together in the measured electrical impedance as follows (Liang *et al.* 1994)

$$Z(\omega) = \frac{V_{in}(\omega)}{I_{out}(\omega)} = \left[ i\omega C_a \left( 1 - \kappa_{31}^2 \frac{Z_a}{Z_S + Z_a} \right) \right]^{-1} \quad (1)$$

where  $C_a$  is the zero-load capacitance of the MFC, and  $\kappa_{31}^2$  is the electromechanical coupling coefficient of the MFC transducer.  $Z$ ,  $Z_S$  and  $Z_a$  are the electrical impedance of the MFC transducer, the mechanical impedance of the host structure, and the mechanical impedance of the MFC transducer, respectively. Assuming that the mechanical impedance of the MFC is invariant, any change in the electrical impedance measured by the MFC transducer can be traced back to the change of the host structure's mechanical properties, allowing monitoring of structural damages within the host structure (Wang and Zhu 2005).

Several damage indices are developed to trace changes of impedance signals (Sun *et al.* 1995, Bhalla *et al.* 2003), and the maximum cross-correlation coefficient is one of them. In this study, the maximum cross-correlation coefficient is used for damage diagnosis and a damage index is defined as follows.

$$DI_{ij} = 1 - CC_{max}(X_i, X_j) \quad (2)$$

$$CC_{max}(X_i, X_j) = \max_{w.r.t. \tilde{\omega}} \left\{ \frac{1}{n-1} \sum_{k=1}^n \frac{(X_i(\omega_k + \tilde{\omega}) - \bar{X}_i)(X_j(\omega_k) - \bar{X}_j)}{\sigma_{X_i} \sigma_{X_j}} \right\} \quad (3)$$

where  $X_i(\omega_k)$  is an impedance value at the  $k^{th}$  frequency point of the impedance signals  $X_i$ ;  $\bar{X}_i$  and  $\sigma_{X_i}$  are the mean and the standard deviation of  $X_i$ , respectively;  $n$  is the total number of frequency measurement points in  $X_i$ ;  $\tilde{\omega}$  is a frequency shift between  $X_i$  and  $X_j$ ; max operation in Eq. (3) finds the highest correlation value between  $X_i$  and  $X_j$  with respect to  $\tilde{\omega}$ . This index has been used to detect structural damage in several applications (Naidu and Soh 2004). However, no certain assertion is made in Eq. (2) that only damage changes the damage index value. Other variations such as changing temperature can also produce changes of the index value. In particular, temperature is known often to cause horizontal shifting of an impedance signal, and this variation can mask the impedance changes caused by structural damage (Yang *et al.* 2008).

Fig. 1 shows the variations of the impedance signals caused by structural damages (corrosion & bolt-loosening) and temperature changes. This Figure illustrates that temperature variations could lead to erroneous diagnosis about the damage state of the structure.

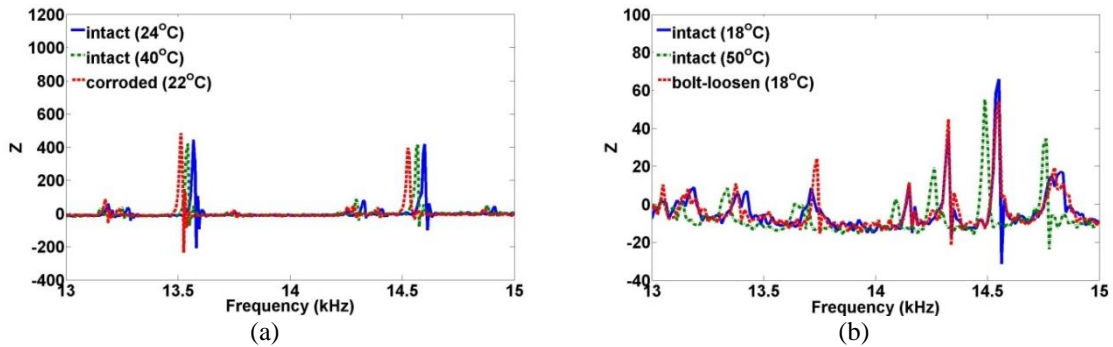


Fig. 1 Changes of the impedance signals caused: (a) by corrosion and temperature variations; and (b) by bolt-loosening and temperature variations

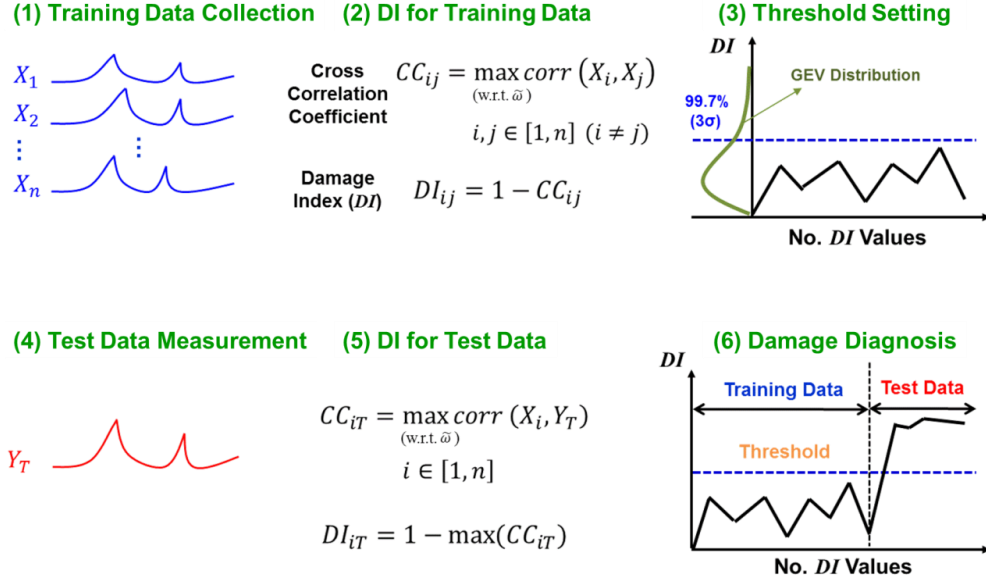


Fig. 2 Overview of temperature compensation process: (1) Multiple impedance signals are recorded under various temperature conditions, and then (2) the damage index values among the training impedance signals are calculated. (3) Next, the statistical distribution of the damage index is estimated using the training data. Because the damage index value obtained from a potential damage condition will fall near the tail of the distribution, GEV statistics is used to focus the modeling effort on the tail of the distribution. Once the statistical model of the training damage index is established, a threshold value corresponding to a user specified confidence level is readily computed for outlier analysis. (4) When a test impedance signal from an unknown condition is obtained, (5) the maximum cross correlations between the test signal and all training signals are computed. And the final damage index is computed between the test signal and a specific training signal that has the largest similarity to the test data. (6) Finally, the damage index value is compared with the threshold value. If the former is larger than the latter, the test signal is considered to be obtained from a damage condition of the structure

To tackle this problem, a temperature compensation technique based on an outlier analysis using GEV statistics is developed (Park and Sohn 2006). Fig. 2 shows the overview of the proposed temperature compensation technique. The detailed procedures are as follows:

- (1) Training Data Collection: Multiple impedance signals are recorded under various temperature conditions of the intact states.
- (2) DI for Training Data: The damage index  $DI_{ij}$  values among the training impedance signals are calculated using Eq. (2).
- (3) Threshold Setting: The statistical distribution of the damage index is estimated using index values obtained from the training data. Because the damage index value obtained

from a potential damage condition will fall near the tail of the distribution, GEV statistics is used to focus the modeling effort on the tail of the distribution. Once the statistical model of the training damage index is established, a threshold value corresponding to a user specified confidence level is readily computed for outlier analysis.

- (4) Test Data Measurement: A test impedance signal is recorded under an unknown state of the structure.
- (5) DI for Test Data: When the test impedance signal becomes available, the maximum cross correlations between the test and all training impedance signals are computed and the final damage index value is computed between the test signal and the specific training signal that is closest to the test signal. In this way, the possibility of false positive indications of damage is reduced.
- (6) Damage Diagnosis: The damage index value is compared with the threshold value. If the former is larger than the latter, the test signal is considered to be obtained from a damage condition of the structure.

### 3. Laser based impedance measurement system

#### 3.1 Overview of the laser based impedance measurement system

Fig. 3 shows an overall schematic of a laser based impedance measurement system adopted in this paper. The system is composed of a data interrogator and an impedance measurement node. It takes advantage of optoelectronics for both signal excitation and measurement. At the data interrogator, an arbitrary waveform such as a broadband chirp signal is generated and converted to a current signal using a metal-oxide-semiconductor field-effect transistor (MOSFET) as a modulated current source driver. Then, the modulated current is applied to the laser diode to vary the laser intensity, and the laser beam is wirelessly transmitted to a photodiode at the impedance measurement node. The photodiode at the impedance measurement node converts the intensity-modulated laser beam into an electric signal and excites a MFC transducer attached to a host structure after amplification. The output current of the MFC transducer is measured using a self-sensing circuit and wirelessly transmitted back to the data interrogator in a similar way to wireless excitation.

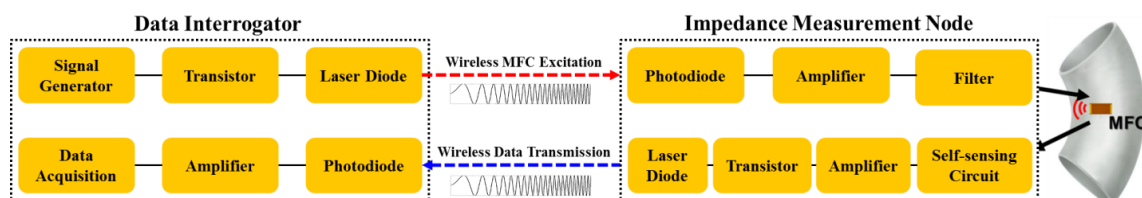


Fig. 3. Overview of the laser based impedance measurement system

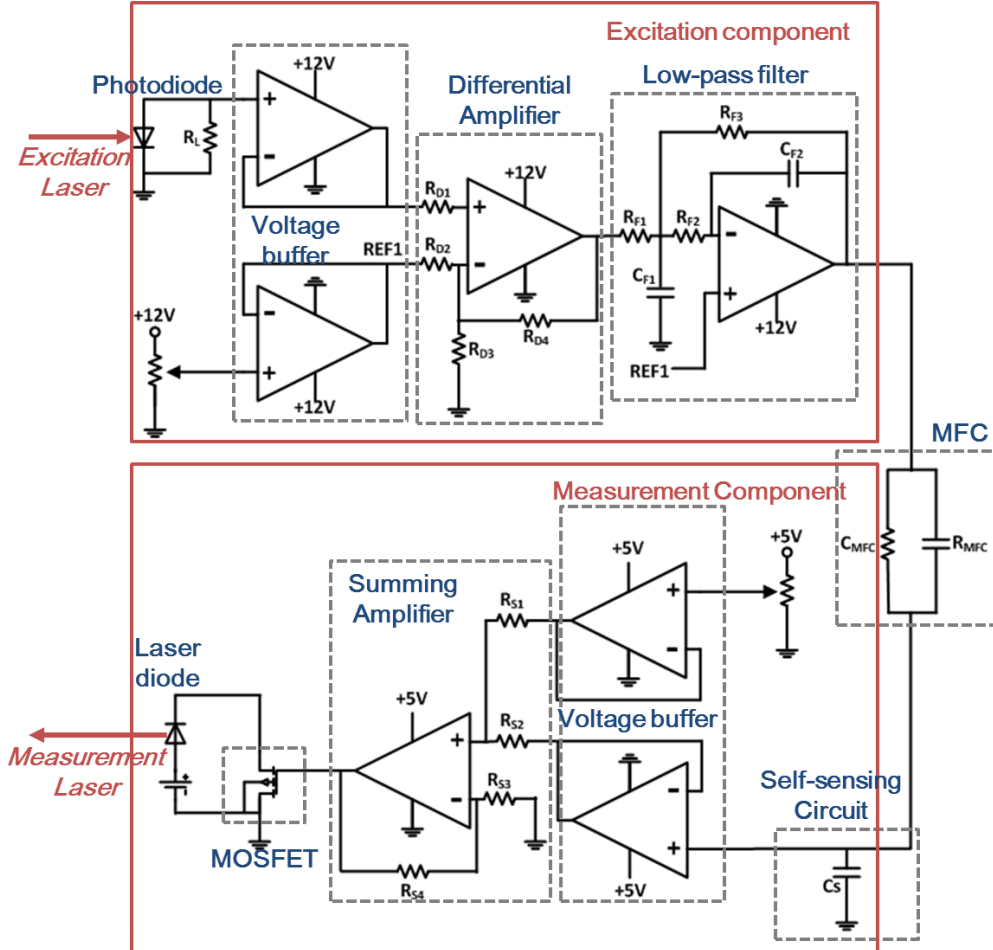


Fig. 4 Equivalent circuit model of the impedance measurement node

Fig. 4 shows the equivalent circuit model of the impedance measurement node. The node is composed of the excitation and the measurement components. The excitation component includes a photodiode, a voltage buffer, a differential amplifier and a low-pass filter. In the measurement component, a self-sensing circuit, a voltage buffer, a summing amplifier, a MOSFET and a laser diode are included. The coupled impedance ( $Z$ ) of the MFC-structure system is defined as the ratio of the excitation voltage ( $V_{IN}$ ) to the output current ( $I_{OUT}$ ) over a specified frequency range. However, when a self-sensing circuit in Fig. 5 is combined with the impedance measurement node, the impedance ( $Z$ ) can be computed at the ratio of the voltage across the MFC ( $V_{IN}-V_{OUT}$ ) to the output current ( $I_{OUT} = V_{OUT}j\omega C_R$ ) at a given driving frequency

$$Z(\omega) = \frac{V_{IN}(\omega) - V_{OUT}(\omega)}{I_{OUT}(\omega)} = \frac{1}{j\omega C_R} \left( \frac{V_{IN}(\omega) - V_{OUT}(\omega)}{V_{OUT}(\omega)} \right) \quad (4)$$

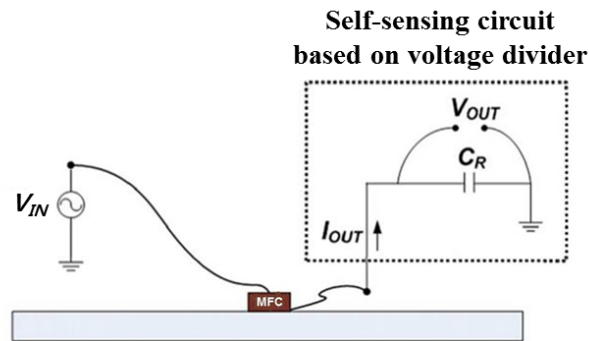


Fig. 5 A self-sensing circuit for impedance measurement (Lee and Sohn 2006)

More details on the working principle of the laser based impedance measurement system can be found in Park et al (Park *et al.* 2012). Note that the power necessary for conversion between electric signals and laser beams at the impedance measurement node is augmented by an additional power supply at this point.

### 3.2 Optimization of the laser based impedance measurement system

In this study, several components are upgraded from the previous ones to improve the performance. First, the wavelength of the excitation laser beam is switched from 1054 nm to 635 nm so that the laser beam becomes visible and can be better aimed at the target photodiode. Accordingly, a new laser diode (HL6322G, Thorlabs) at 635 nm and a photodiode (FDS100, Thorlabs) with a working wavelength range of 350 nm to 1100 nm are chosen.

Because of the nonlinear characteristics of the MOSFET, the laser diode and the photodiode, there can be distortion between the ideal input signal from the signal generator and the actual excitation signal applied at MFC or between the true measured signal from the self-sensing circuit and the final response signal measured by the data interrogator. To address this nonlinearity issue, the linearity between laser and electricity conversion is improved by using components (HL6322G, Thorlabs, FDS100, Thorlabs, MMFT960T, Motorola) with improved linear characteristics and restricting inputs to each component within a localized linear region.

Fig. 6 compares an ideal 50 kHz sine signal generated from the arbitrary waveform generator ( $V_{AWG}$ ) with the actual input signal applied to the MFC ( $V_{IN}$ ). To focus on the shape comparison, each signal is normalized with respect to its maximum value. DC component in  $V_{IN}$  is removed, and the time delay between them is eliminated. Indeed, there exists 0.65  $\mu$ s time delay between  $V_{AWG}$  and  $V_{IN}$ , and that is most likely attributed to the photodiode and laser diode characteristics. However, the time delay is invariant of the driving frequency and MFC characteristics. Also, since the amplifiers in the impedance measurement node are powered by a single 12 V DC power supply, a DC component around 6 V is added to  $V_{IN}$ . However, this DC component does not affect the MFC operation because MFC is not responsive to a low frequency input near a DC level. Fig. 6 illustrates that the phase distortion is negligible in the developed system.

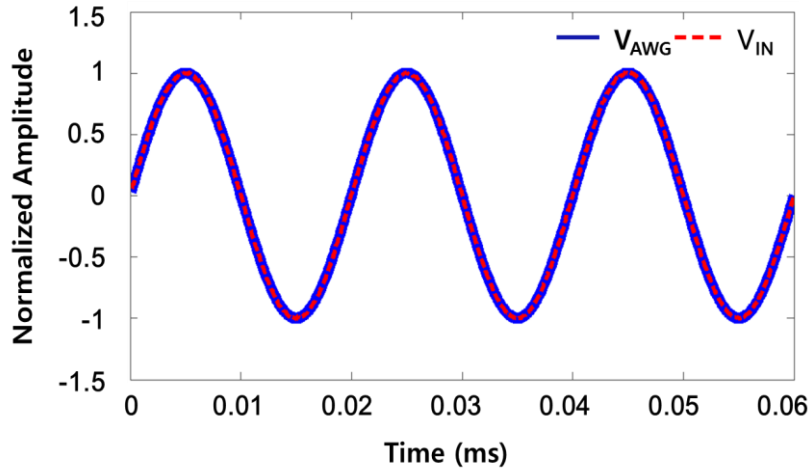


Fig. 6 Comparison of  $V_{AWG}$  from the signal generator and  $V_{IN}$  applied to the MFC at the impedance measurement node after amplitude normalization, time shifting and DC removing

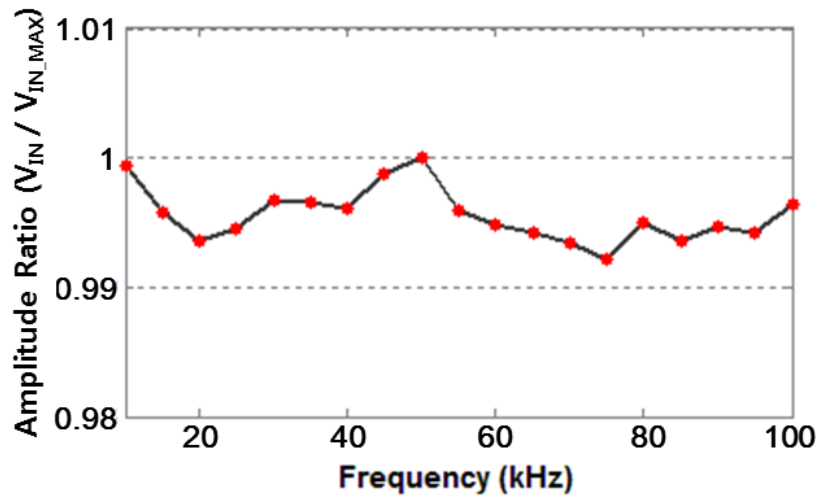


Fig. 7 Variation of  $V_{IN}$  amplitude with respect to the driving frequency

Next, the driving frequency of  $V_{AWG}$  is varied from 10 kHz to 100 kHz, and the amplitude ratio of  $V_{IN}$  to  $V_{IN\_MAX}$  is plotted in Fig. 7. Here, the  $V_{IN\_MAX}$  is defined as the maximum value of  $V_{IN}$  between 10 kHz and 100 kHz. It is confirmed that the amplitude of  $V_{IN}$  is consistent throughout the investigated frequency range, and the amplitude variance is confined to be less than 1%.

Finally, the peak voltage of  $V_{IN}$  is increased from  $5 V_{pp}$  in the previous version to  $12 V_{pp}$  so that a larger excitation force can be applied to the MFC. Furthermore, a low-pass filter is used to remove high-frequency noise above 200 kHz.

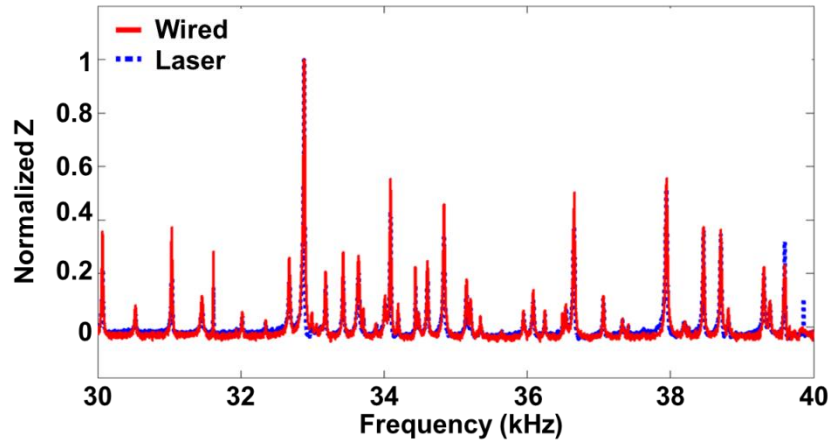


Fig. 8 Comparison of the impedance signals obtained by the conventional wired (solid) and proposed laser based (dashed) impedance measurement systems

### 3.3 Comparison with a conventional wired impedance measurement system

The performance of the laser based impedance measurement system is compared with a conventional wired impedance measurement system. Experimental tests are conducted on a carbon steel elbow pipe (SS41) with an outer diameter of 125 mm and a wall thickness of 4.4 mm. A MFC transducer with dimensions of  $28 \times 14 \times 0.02 \text{ mm}^3$  is attached to the elbow pipe. An Agilent 4294A precision impedance analyzer is used for wired impedance measurement. More details on the test setup and the laser based impedance measurement system are described in the next section.

The impedance signals measured by the conventional wired and the proposed laser based impedance measurement systems are shown for the frequency range of 30 kHz to 40 kHz in Fig. 8. The solid and dotted lines denote the impedance signals obtained by the wired and laser based impedance measurement systems, respectively. Two signals are normalized so that their peak values are equal to one. The comparison shows a good agreement.

## 4. Corrosion detection in an elbow pipe

### 4.1 Test setup

Fig. 9 shows the experimental setup and the test specimen. At the data interrogator of the laser based impedance measurement system, a NI PXI system, which integrates a 12 bit arbitrary waveform generator (AWG), a 16 bit high-speed signal digitizer (DIG), and a LABVIEW® control program, is used to generate and acquire electric signals. A  $0.28 \text{ V}_{pp}$  chirp input ranging from 10 kHz to 50 kHz is generated using the AWG. A modulated laser beam is generated using a laser diode (HL6322G, Thorlab) and focused onto a photodiode (FDS100, Thorlab) at the impedance measurement node. The converted electrical input is amplified and filtered, and a  $6.0 \pm 4.0 \text{ V}$  signal is applied to the MFC. Then, the output response of the MFC is measured using a

self-sensing circuit, converted into a laser beam, transmitted back, collected by the other photodiode (PDA100A-EC, Thorlab) and the digitizer (DIG) at the data interrogator, and the impedance is computed. The travel distance of the laser beams is set to 1 m, and additional long range power and data transmission with laser beams are also successfully performed up to 10 m although they are not reported here.

The specimen is a carbon steel elbow pipe (SS41) with 125 mm of outer diameter and 4.4 mm of wall thickness. MFC transducers (Smart Material Co. Ltd) of  $28 \times 14 \times 0.02 \text{ mm}^3$  are installed as shown in Fig. 9 to measure the impedance signals through the proposed laser based impedance measurement system. Among these MFC transducers attached on the pipe surface as shown in Fig. 9, representative results from MFC 1 are reported in this study.

Temperature effects on the impedance measurement are investigated first as described in section 2. The training impedance data sets are collected from the intact condition of the specimen at  $0^\circ\text{C}$ ,  $10^\circ\text{C}$ ,  $20^\circ\text{C}$ ,  $30^\circ\text{C}$ ,  $40^\circ\text{C}$ , and  $50^\circ\text{C}$  with 30% constant humidity. By using a temperature chamber, temperature and humidity are controlled. The temperature of the test specimen's surface is measured by a thermocouple. For corrosion test, 5M sulfuric acid solution of 30 mL is used. The impedance signals are measured at every 12 hours for a total of 48 hour duration. To monitor the thickness change of the specimen, an ultrasonic thickness gauge (SC20, Picosonic) is used. The thickness decreases about 0.05 mm per every 12 hours, and the final thickness is about 4.20 mm.

#### 4.2 Test results

Table 1 lists the impedance signals obtained under varying temperature and pipe thickness conditions. The first 60 data sets (#1-60) are obtained from varying temperature conditions of the intact specimen, and used as training data sets for the building of the outlier analysis model. As temperature increases, the impedance peaks are shifted to the left as mentioned in section 2. Additional 20 data sets (#61-80) are obtained from the intact condition for false alarm tests. And the last data sets (#81-120) are obtained at varying temperature and corrosion conditions. To distinguish corrosion effect from temperature variations, the temperature compensation algorithm previously described is applied.

Fig. 10 shows the damage diagnosis for the testing data sets (#61-120). The threshold value corresponding to a 97% confidence interval is set to 0.13 by fitting a GEV distribution to the damage index values obtained from the training data sets. The damage index values increase as the corrosion progresses.

Table 1 Description of training and test data sets obtained from a curved pipe specimen

	Data	Thickness	Temp.( $^\circ\text{C}$ )		Data	Thickness	Temp.( $^\circ\text{C}$ )
<b>Training</b>	1~10	t=4.40mm	0	<b>Testing</b>	61~70	t=4.40mm	13
	11~20	t=4.40mm	10		71~80	t=4.40mm	24
	21~30	t=4.40mm	20		81~90	t= 4.35mm	27
	31~40	t=4.40mm	30		91~100	t= 4.30mm	21
	41~50	t=4.40mm	40		101~110	t= 4.25mm	22
	51~60	t=4.40mm	50		111~120	t=4.20mm	29

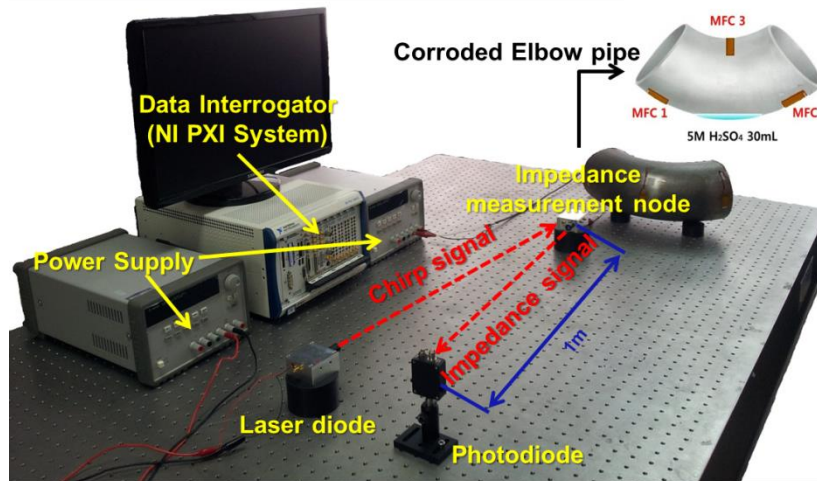


Fig. 9 Experimental setup and test specimen for corrosion detection

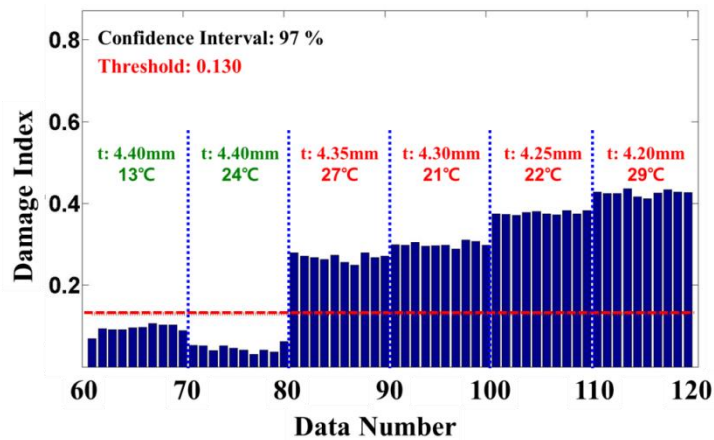


Fig. 10 Damage diagnosis using an outlier analysis under temperature variations

## 5. Bolt-loosening detection in a flange connected elbow pipe

### 5.1 Test setup

Fig. 11 shows the experimental setup and the test specimen. The data acquisition system same as the previous corrosion test is used. The specimen consists of the same carbon steel elbow pipe and two carbon steel straight pipes (SS41), and they are connected by bolts and welding. Four MFC transducers are attached on the pipe surface as shown in Fig. 11. Among these MFC

transducers, impedance signals are measured from MFC 4, and temperature effect is compensated as before. Bolt-loosening is simulated by loosening one out of eight bolt by a quarter turn using a spanner. The rest of the test setup is identical to the previous experiment.

### 5.2 Test results

Table 2 shows the list of the impedance signals obtained under varying temperature. The first 60 data sets (#1-60) are obtained from varying temperature conditions of the intact structure and used to build the statistical model. The additional 10 data sets (#61-70) obtained from the intact condition are used for false alarm tests. The last data sets (#71-130) are obtained under changing temperature conditions after bolt-loosening.

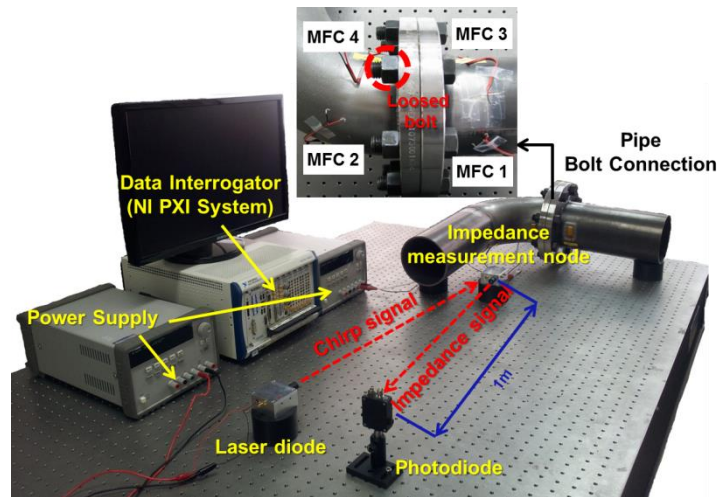


Fig. 11 Experimental setup and test specimen for bolt-loosening detection

Table 2 Description of training and test data sets obtained from a flange connected elbow pipe

	Data	State	Temp.( $^{\circ}$ C)		Data	State	Temp.( $^{\circ}$ C)
<b>Training</b>	1~10	Intact	0	<b>Testing</b>	61~70	Intact	25
	11~20	Intact	10		71~80	Bolt-loosen	18
	21~30	Intact	20		81~90	Re-tighten	18
	31~40	Intact	30		91~100	Bolt-loosen	23
	41~50	Intact	40		101~110	Re-tighten	23
	51~60	Intact	50		111~120	Bolt-loosen	20
					121~130	Re-tighten	20

Fig. 12 shows the damage diagnosis for the testing data sets (#61~80). The threshold value corresponding to a 97% confidence interval is set to 0.17 by fitting a GEV distribution to the damage index values obtained from the training data sets. The damage index values increase as bolt-loosening progressed.

Additional tests are performed by repeating bolt-loosening and tightening as shown in Fig. 13. The impedance signals are measured after a quarter turn of one of the bolts, and measured again after fully re-tightening the bolt. It is confirmed that the damage index value increases after bolt loosening, recovers back close to the initial value after re-tightening. This bolt loosening and tightening experiment is repeated in three consecutive days, and consistent results are observed except a slightly increase of the damage index when the bolt is re-tightened.

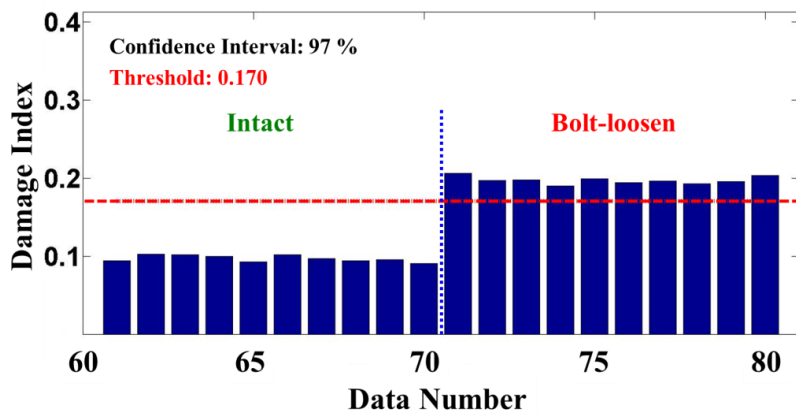


Fig. 12 Damage diagnosis using an outlier analysis under temperature variations

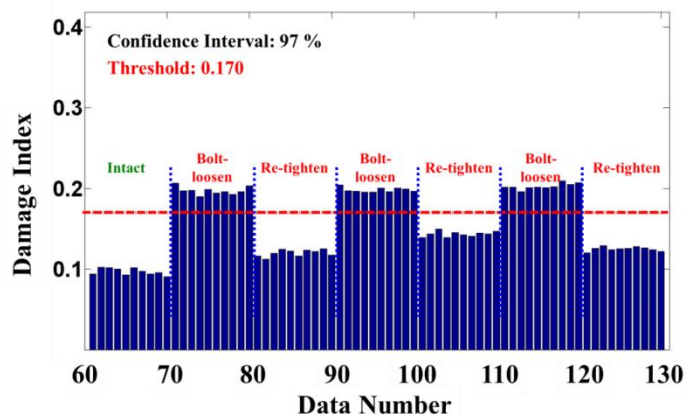


Fig. 13 Damage diagnosis under repeated bolt-loosening tests

## 6. Conclusions

This study examines the applicability of a laser based impedance measurement system to continuous monitoring of corrosion and bolt-loosening damages in pipe structures under temperature variations. For impedance measurement, a laser based impedance measurement system is introduced. First, a modulated laser beam is radiated to a photodiode connected to a MFC transducer on a target structure. Then, the photodiode converts the laser beam into an electric signal, and applied to the MFC transducer for ultrasonic excitation. The corresponding impedance signals are measured, re-converted into a laser beam, and radiated back to the other photodiode located in a data interrogator. To minimize erroneous diagnosis under temperature variations, measured impedance signals are treated with an outlier analysis and a generalized extreme value statistics to reliably signal off structural damage. Validation of the proposed technique is carried out to detect corrosion and bolt-loosening in lab-scale carbon steel elbow pipes under varying temperatures. It has been demonstrated that the proposed technique has a potential to be used for structural health monitoring of pipe structures. Follow-up studies are warranted to improve the performance of the proposed technique. First, the proposed technique is only tested for a lab-scaled specimen, but the robustness of the proposed technique needs to be more thoroughly investigated using more complex and realistic pipe structures. Second, besides corrosion and bolt loosening, cracking due to repeated loading and local buckling is another critical failure mode for pipe structures. However, the crack damage is not investigated in this study. Finally, the current outlier analysis takes into account only temperature changes. Real pipe structures are also subjected to other operational variations such as ambient vibrations, varying pipe pressure, and changing fluid speed, etc. Multiple varying conditions should be considered in future studies.

## Acknowledgements

This research was supported by Mid-career Researcher Program at the National Research Foundation of Korea (NRF) funded by the Ministry of Education, Science and Technology (No. NRF-2010-0017456) and a grant from the EEWS Research Project of the office of KAIST EEWS Initiative (No. EEWS-2013-N01130015).

## References

- Ayres, J.W., Lalonde, F., Chaudhry, Z. and Rogers, C.A. (1998), "Qualitative impedance-based health monitoring of civil infrastructures", *Smart Mater. Struct.*, **7**(5), 599-605.
- Azevedo, C.R.F. (2007), "Failure analysis of a crude oil pipeline", *Eng. Fail. Anal.*, **14**(6), 978-994.
- Bhalla, S., Naidu, A.S.K. and Soh, C.K. (2003), "Influence of structure-actuator interactions and temperature on piezoelectric mechatronic signatures for NDE", *Proceedings of the SPIE Conference on Smart Materials, Structures, and Systems*, San Diego, USA, March.
- Bhalla, S. and Soh, C.K. (2004), "High frequency piezoelectric signatures for diagnosis of seismic/blast induced structural damages", *NDT & E Int.*, **37**(1), 23-33.
- Chaudhry, Z. and Ganino, A.J. (1994), "Damage detection using neural networks: an initial experimental study on de-bonded beams", *J. Intel. Mat. Syst. Str.*, **5**, 585-589.
- Giurgiutiu, V., and Zagari, A.N. (2002), "Embedded self-sensing piezoelectric active sensors for online structural identification", *J. Vib. Acoust.*, **124**(1), 116-125.

- Giurgiutiu, V. and Zagari, A. N. (2005), "Damage detection in thin plates and aerospace structures with the electro-mechanical impedance method", *Struct. Health Monit.*, **4**(2), 99-118.
- Grisso, B.L. and Inman, D.J. (2008), "Autonomous hardware development for impedance-based structural health monitoring", *Smart Struct. Syst.*, **4**(3), 305-318.
- Hamzeloo, S.R., Shamsirsaz, M. and Rezaei, S.M. (2012), "Damage detection on hollow cylinders by Electro-Mechanical Impedance method: Experiments and finite element modeling", *Comptes Rendus Mecanique*, **340**, 668-677.
- Kim, M., Kim, E., An, Y., Park, H., Sohn, H. (2011) "Reference-free impedance based crack detection in plates", *J. Sound Vib.*, **330**(24), 5949-5962.
- Krishnamurthy, K., Lalonde, F. and Rogers, C.A. (1996), "Effects of temperature on the electrical impedance of piezoelectric sensors", *Proceedings of the SPIE Conference on Smart Materials, Structures, and Systems*, San Diego, USA, March.
- Lawson, K. (2005), "Pipeline corrosion risk analysis – an assessment of deterministic and probabilistic methods", *Anti-Corros. Method. M.*, **52**(1), 3-10.
- Lee, S. and Sohn, H. (2006) "Active self-sensing scheme development for structural health monitoring", *Smart Mater. Struct.*, **15**(6), 1734-46.
- Liang, C., Sun, F.P. and Rogers, C.A. (1994), "Coupled electro-mechanical analysis of adaptive material system-determination of the actuator power consumption and system energy transfer", *J. Intel. Mater. Syst. Str.*, **5**(1), 12-20.
- Lim, H., Kim, M., Sohn, H. and Park, C. (2011), "Impedance based damage detection under varying temperature and loading conditions", *NDT&E Int.*, **44**(8), 740-750.
- Mascarenas, D.L., Todd, M.D., Park, G., Farrar, R. (2007), "Development of an impedance-based wireless sensor node for structural health monitoring", *Smart Mater. Struct.*, **16**(6), 2137-2145.
- Min, J., Park, S., Yun, C. and Song, B. (2010), "Development of a low-cost multifunctional wireless impedance sensor node", *Smart Struct. Syst.*, **6**(5), 689-709.
- Naidu, A.S.K. and Soh, C.K. (2004), "Damage severity and propagation characterization with admittance signatures of piezo transducers", *Smart Mater. Struct.*, **13**(2), 393-403
- Papadakis, G.A. (1999), "Major hazard pipelines: a comparative study of onshore transmission accidents", *J. Loss Prevent. Proc.*, **12**(1), 91-107.
- Park, H. and Sohn, H. (2006), "Parameter estimation of generalized extreme value distribution for structural health monitoring", *Probabilist. Eng. Mech.*, **21**(4), 366-376.
- Park, H., Sohn, H., Yun, C., Chung, J. and Kwon, I. (2012), "A wireless guided wave and impedance measurement using laser and piezoelectric transducers", *Smart Mater. Struct.*, **21**(3), 1-10.
- Sun, F., Chaudhry, Z. and Rogers, C.A. (1995), "Automated real-time structure health monitoring via signature pattern recognition", *Proceedings of the SPIE Conference on Smart Materials, Structures, and Systems*, San Diego, USA, March.
- Thien, A.B., Chiamori, H.C., Ching, J.T., Wait, J.R. and Park, G. (2007), "The use of macro-fibre composites for pipeline structural health assessment", *Struct. Control Health Monit.*, **15**(1), 43-63.
- Wang, D.S. and Zhu, H.P. (2005), "Wave propagation based multi-crack identification in beam structures through anti-resonance information", *Key Eng. Mater.*, **293**, 557-564.
- Yang, Y., Hu, Y. and Lu, Y. (2008), "Sensitivity of PZT impedance sensors for damage detection of concrete structures", *Sensors*, **8**, 327-346.
- Zhang, Y., Zhou, Y., Xu, F. and Li, H. (2012), "Damage detection of pipes based on PVDF", *Appl. Mech. Mater.*, **198-199**, 158-161.
- Zou, Y., Tong, L. and Steven, G.P. (2000), "Vibration-based model-dependent damage (delamination) identification and health monitoring for composite structures – a review", *J. Sound Vib.*, **230**(2), 357-378.